Eur. Phys. J. B **51**, 65–73 (2006)
DOI: 10.1140/epjb/e2006-00188-7

THE EUROPEAN PHYSICAL JOURNAL B

Effects of size and surface anisotropy on thermal magnetization and hysteresis in the magnetic clusters

Z. Huang[1,a], Z. Chen[1], S. Li[1], Q. Feng[1], F. Zhang[2], and Y. Du[2]

[1] Department of Physics, Fujian Normal University, Fuzhou, 350007, P.R. China
[2] National Laboratory of Solid State Microstructures, Nanjing University, Nanjing 210093, P.R China

Received 20 August 2005 / Received in final form 18 January 2006
Published online 31 May 2006 –

Abstract. Based on Monte Carlo simulation, the spin configurations, thermal magnetization and hysteresis loops of the clusters coated by the surface shell with radial anisotropy are studied. Interestingly, a new multidomain containing a few of subdomains whose easy directions are along those of the configurational anisotropy, a magnetization curve in steps and a first order phase transition from the single domain to the multidomain in the thermal and field magnetization processes, are found, which is as a result of the interplay of the configurational anisotropy, the size effect, the surface anisotropy, the applied field and the thermal fluctuation. In this first order transition, we find a critical temperature, a critical surface anisotropy and a critical size. The simulated temperature dependence of the coercivity of the cluster with the surface anisotropy can be fitted by $H_c(T) = H_c(0)(1 - C_\alpha T^\alpha)$ with low value of α, which explains well the experimental results of the nanoparticles. Moreover, it is found that the hysteresis loops and coercivity are strongly affected by the cluster size and the thickness of the surface layer.

PACS. 75.75.+a Magnetic properties of nanostructures – 75.40.Mg Numerical simulation studies – 75.60.Ej Magnetization curves, hysteresis, Barkhausen and related effects – 75.60.Jk Magnetization reversal mechanisms

1 Introduction

The magnetic properties of nanoparticles and clusters have been interesting subjects for the last two decades due to their important technological applications and their novel characters that are quite different from those of bulk materials. Surface effects for the clusters are of great importance since they dominate magnetic properties and become more important with reducing size of the particle. For clusters with a radius of several nanometers, the picture of a single-domain magnetic particle in which all spins point into the same direction and the coherent relaxation processes are produced is not valid as the surface effects become really crucial. A large surface effects and strong anisotropy field have been found in a lot of nanoparticles [1–12]. For example, Mossbauer spectra and magnetization measurements for the cobalt, nickel ferrite, γ-Fe_2O_3 and other nanoparticles have shown that the magnetization and spin configuration are strongly influenced by the surface and size effects. Moreover, it has also been found that the anisotropy energy per unit volume increases by more than an order of magnitude for small clusters compared to the bulk value [11,12]. Those experimental facts have given rise to great interest in theory [13–24]. Each spin at the surface has a lower symmetry than that in the bulk, and the surface anisotropy may arise from the interplay between the spin-orbit coupling and the local crystalline electric field. The crystal symmetry and the coordination number at the surface of the clusters are reduced and consequently the anisotropy is expected to be stronger. Moreover, it is assumed that the anisotropy at the surface is radial based on the symmetry at the surface of the clusters and experimental results. Based on Heisenberg model, the hysteresis behavior of small ferromagnetic and ferrimagnetic clusters with large surface anisotropy have been studied by solving the Landau-Lifshitz equations or Monte Carlo method [14,18–24]. It was observed that the coercivity increases with decreasing cluster size and a step effect exists in the loops due to the reversal of surface spins at different fields.

In our previous studies [24,25], magnetization, Curie temperature, hysteresis, coercivity, natural angle and energy distribution for the clusters with zero and finite uniaxial anisotropy were calculated using Monte Carlo simulation. The hysteresis and the spin configurations in different magnetization progress reveal the existence of an easy magnetization direction and an anisotropy resulting from the spin configurations. The simulated natural angle and energy distribution in the clusters were obtained, which proves further the existence of the configurational

[a] e-mail: zghuang@fjnu.edu.cn

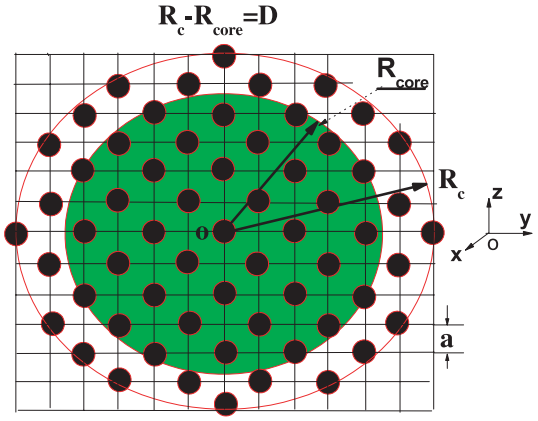

Fig. 1. A cross-section schematic of the atomic arrangement in the spherical cluster.

anisotropy in the clusters. The hysteresis loops and thermal coercivities were well explained by the spin configuration, the natural angle and energy distribution. In this work, we study further the influence of the surface anisotropy on the magnetic properties of the clusters with small or zero core uniaxial anisotropy. The magnetization process is treated quasistatically with emphasis on the influences of the cluster size and the magnitude of surface anisotropy on the spin configurations, thermal magnetization and hysteresis loops. Of particular interest is the existence of a first order phase transition from the single domain to the multidomain in the thermal and field magnetization processes due to the interplay of the configuration anisotropy, the size effect, the surface anisotropy (K_s), the applied field and the thermal fluctuation. For the clusters with $K_s = 10$, $N = 2123$ and 249, the thermal coercivity can be fitted by $H_c(T) = H_c(0)(1 - C_\alpha T^\alpha)$, which is consistent with the experimental results of the nanoparticles. The changes of the hysteresis loops and coercivity with the cluster size and the thickness of the surface layer demonstrate that the reversal mode is strongly influenced by the reduced coordination and disorder at the surface.

2 Model and simulation technique

The atomic spins are placed on the sites of an fcc lattice. A cross-section schematic of the atomic arrangement in the spherical cluster is shown in Figure 1. It is assumed that the cluster is a spherical shaped particle with radius R_c. The cluster is divided into both parts: core and surface. The radius of the core is R_{core}, and the thickness of the surface shell, $R_c - R_{core}$, is D. In the simulation, a is set as half of the lattice constant and is taken as the reduced unit ($a = 1$). The similar core and shell structure has been used by Zianni and Trohidou [27]. The numbers of the atoms corresponding to $R_c = 10$, 9, 8, 7, 6, 5, 3.75, 3 for the fcc clusters are 2123, 1505, 1061, 683, 459, 249, 135, 55, respectively. We consider classical Heisenberg exchange interactions between the spins in the cluster in a magnetic field. The system Hamiltonian of the cluster is

$$H_s = -\sum_{\langle ij \rangle} J_{ij}\, \vec{S}_i \cdot \vec{S}_j - \sum_i K_\alpha \left(\vec{S}_i \cdot \vec{k}_i\right)^2 - H \sum_i S_i^z \tag{1}$$

where $\sum_{\langle ij \rangle}$ is performed over the spin pairs at nearest-neighbor (NN) sites i and j with exchange interaction J_{ij}, K_α means the anisotropy constant of the core K_b or of the surface K_s depending on whether site i belongs to the core or to the surface. For fine particles there is some evidence that the easy axis is along the z direction [26]. Hence, $\vec{k}_i$ in the core is taken to be along the z direction. $\vec{k}_i$ in the surface is taken to be perpendicular to the surface of the cluster, and is along the direction from the center spin site to the considered surface site. We let $|\vec{S}_i| = 1$. The exchange interaction J_{ij} in equation (1) between the sites i and j is taken as J. Here, J is used as unit of temperature and energy, and let $J = 1$. Free boundary conditions are applied in all directions.

The Monte Carlo method for a classical Heisenberg system has been found in literatures [24,28]. In the simulation, the first 10^4 MC steps per spin were discarded for equilibrium and thermal averages were made with next 10^4 steps. In thermal average process, we started to store the simulated parameter values separated by every 20 MC steps to break correlation between successive configurations. Based on experimental measurement procedure of the zero field-cooled and field-cooled system, we started from a random configuration in the high temperature region and cooled quasicontinuously down to measured temperature of the system without or with the magnetic field at a constant temperature step $T = -0.05{-}0.1$. 400 MC steps were performed at each temperature. Then, the hysteresis loops were computed by starting from a demagnetized state at $H = 0$ and increasing quasicontinuously the magnetic field to H_m, then decreasing to $-H_m$, and increasing to $+H_m$, during which ΔH is taken as 0.02–0.05 and the magnetization was averaged over ∼2000 MC steps at each field.

3 Simulated results and discussion

3.1 Thermal magnetization

The core, surface and total magnetizations of the clusters for $N = 2123$ with $K_b = 0$, $K_s = 0$, 10 as a function of the temperature are shown in Figure 2, respectively. It is found that the magnetization curve in the surface is different from that in the core. For $K_s = 0$, the reduction rate of the magnetization with increasing temperature for the surface is larger than one for the core. Based on the Bloch' $T^{3/2}$ law, $M(T) = M(0)(1 - BT^{3/2})$, it is found that the $T^{3/2}$ law is well satisfied for the thermal magnetization curves of the surface, the core and the total cluster. It is obtained that $B_s = 0.0468$, $B_b = 0.0245$, which reveals clearly the surface effect. For $K_s = 10$, the magnetization of the surface is much lower than that of

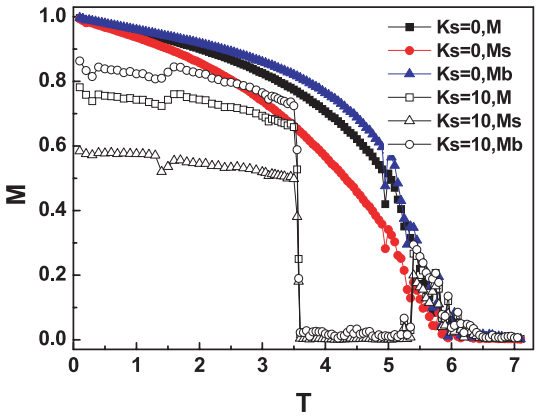

Fig. 2. The total, core and surface magnetizations of the cluster with $N = 2123$ and $K_b = 0$, $K_s = 0$, 10 as a function of the temperature.

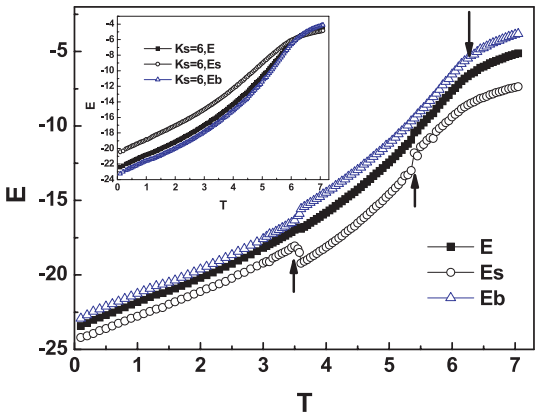

Fig. 3. The temperature dependence of the core, surface and total energies of the cluster for $N = 2123$ with $K_b = 0$, $K_s = 10$. The inset shows that with $K_b = 0$, $K_s = 6$.

the core at $0 < T < 3.3$, which demonstrates the disorder of the surface spins. The temperature dependences of the energies of the core, the surface and the total cluster for the same cluster with $K_b = 0$, $K_s = 10$ are shown in Figure 3, and the inset shows those with $K_b = 0$, $K_s = 6$. Figures 4a and 4b show the thermal dependences of the specific heat and susceptibility for the same cluster with $K_b = 0$, $K_s = 10$, respectively. Figures 2–4 indicate evidently that both first and second order phase transitions exist in the cluster with $K_b = 0$, $K_s = 10$. In order to explain the above transitions, the corresponding spin configurations at different temperature are shown in Figures 5a, 5b, 5c and 5d. As $T < 0.3$, the spin configuration as found in Figure 5a ($T = 0.2$) is that the spins of the core are collinear and along z axis while those of the surface are misaligned. As $0.3 \leq T < 3.3$, the spin configuration as seen in Figure 5b ($T = 2.0$) is that the spins of the core align the easy axis which results from the configurational anisotropy and has been discussed in detail in our previous work [25]. At $T = 3.5$ and 5.5, a first order transition emerges due to the change of the magnetization state from the single domain to multidomain. When the temperature is between 3.3 and 5.5, the spin configuration is a multidomain structure with several subdomains whose magnetization directions are along two symmetric easy axes [24], as seen in Figure 5c ($T = 4.0$). Comparing the thermal energy for $K_s = 6$ with that for $K_s = 10$ as shown in Figure 3, one can clearly note that the multidomain is mainly attributed to the reduction of the energy of the surface. Although the energy of the core in the multidomain increases slightly, the total energy of the cluster in the multidomain is lower than one in the single domain

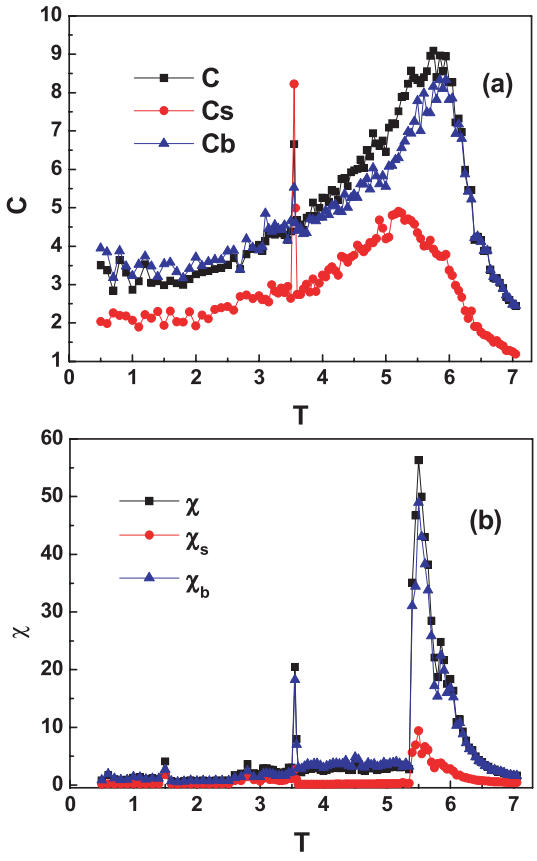

Fig. 4. The thermal dependence of the specific heat (a) and susceptibility (b) for $N = 2123$ with $K_b = 0$, $K_s = 10$.

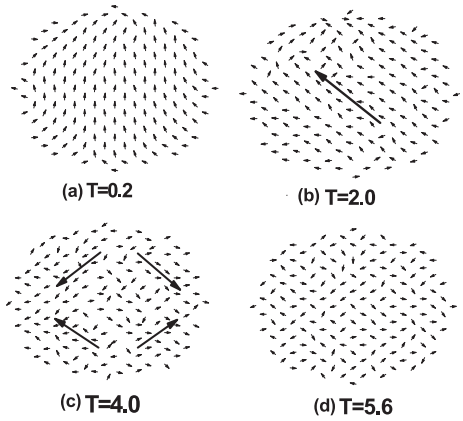

Fig. 5. The spin configurations of the cluster for $N = 2123$ with $K_b = 0$, $K_s = 10$, (a) $T = 0.2$; (b) $T = 2.0$; (c) $T = 4.0$ and (d) $T = 5.6$, respectively.

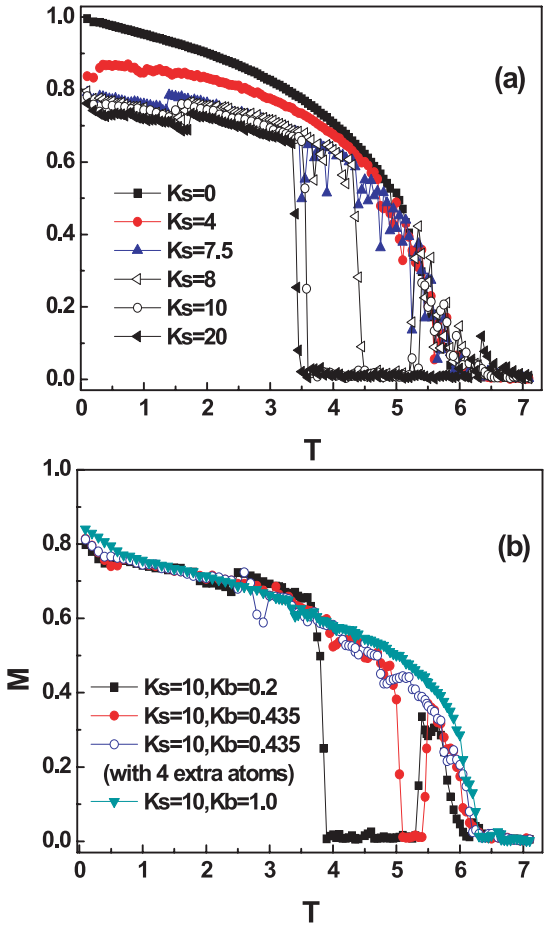

Fig. 6. The thermal magnetization of the cluster, (a) for $N = 2123$ with $K_b = 0$, $K_s = 0$, 4, 7.5, 7.8, 10, 20, respectively; (b) for $N = 2123$ with $K_b = 0.2$, 0.435, 1.0, $K_s = 10$, and for $N = 2123 + 4$ with $K_b = 0.435$, respectively.

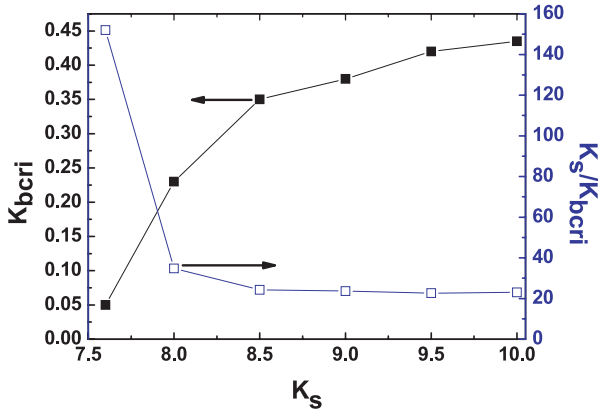

Fig. 7. The critical core anisotropy K_{bcri} and K_s/K_{bcri} as a function of surface anisotropy K_s for the clusters with $N = 2123$.

due to the distinct decrease of surface energy. Moreover, the simultaneous transition of demagnetizations reveals the strong correlation between the surface and core spins. This phase transition is similar to that from the flower state to the vortex state in ferromagnetic cubes and patterned square magnetic nanostructure [29,30]. The underlying cause of such transition is the interplay of the configurational anisotropy [24,31,32], the surface anisotropy and the thermal fluctuation. As the temperature increases from 5.5 to 7, the cluster is firstly at a weak ferromagnetic state and then goes through a second order phase transition, reaching a paramagnetic state. Figure 6a shows the thermal magnetization of the cluster for $N = 2123$ with $K_s = 0$, 4, 7.5, 8, 10, 20, respectively. It is found that the magnitude of the surface anisotropy has an important influence on the thermal magnetization, and there is a critical magnitude of the surface anisotropy K_{scri} (=7.5). As $K_s < K_{scri}$, the first order phase transition disappears. Figure 6b shows the thermal magnetization of the cluster for $N = 2123$ with $K_b = 0.2$, 0.435, 1.0, $K_s = 10$, and for $N = 2123 + 4$ with $K_b = 0.435$, respectively. Here, for $K_b = 0.435$ and $K_s = 10$, we calculated the results of the cluster with and without the extra-atoms (4). Those extra 4 atoms were added on the outside of the surface that locates in the direction of $+X$ axis. From Figure 6b, it is found that the value of the core anisotropy K_b has an evident role on the thermal magnetization, and there exists a critical value of the core anisotropy. For $K_s = 10$, $K_{bcri} = 0.435$. As $K_b > K_{bcri}$, the first order phase transition disappears. Moreover, the values of K_{bcri} and K_s/K_{bcri} as a function of K_s for the clusters with $N = 2123$, are shown in Figure 7, respectively. From the figure, it is found that the value of K_{bcri} increases with the enhancement of K_s, while the value of K_s/K_{bcri} decreases with increasing magnitude of K_s. However, the changes of values of K_{bcri} and K_s/K_{bcri} with K_s are gentle for $K_s > 8.5$. Now, we analysis further in detail the spin configurations for $K_s = 10$, $K_b = 0.2$ and 1.0 as seen in Figure 6b, especially those corresponding to the existence of the first order transition. It is observed that the spin configurations at different temperature ranges for $K_s = 10$, $K_b = 0.2$ in Figure 6 are similar to those in Figure 5. Moreover, we made the frequency counting of the spin orientation on the spin configurations. Figures 8a and 8b shows the typical spin orientation distributions at $T = 0.1$, 1.5, 3.8, 3.9, 4.0, 5.6 for $N = 2123$, $K_s = 10$, $K_b = 0.2$ and 1.0, respectively. As seen in Figure 8a, for $K_b = 0.2$, the spin orientation distributions can be described with four temperature regions: region (I) with $T < 0.3$, there exists only peak in the spin orientation distributions and the site of the peak locates at $\theta \approx \pi/2$, which means that the spins prefer to be along Z-axis; region (II) with $0.3 \leq T \leq 3.8$, there exists also only peak, but the site of the peak locates at $\theta \approx 0.70$, which indicates the spins prefer to align the easy axis of the configurational anisotropy as found in Figure 5b; region (III) with $3.8 < T < 5.4$ (multidomain region), there exist four peaks that are almost symmetric along zero-axis ($\theta \approx 0$), which means further that the spins are along two symmetric easy axes (corresponding to four symmetric directions); region (IV) with $5.4 \leq T < T_c$ (Curie temperature), there exist almost two peaks with positive or negative angles, which means that the order

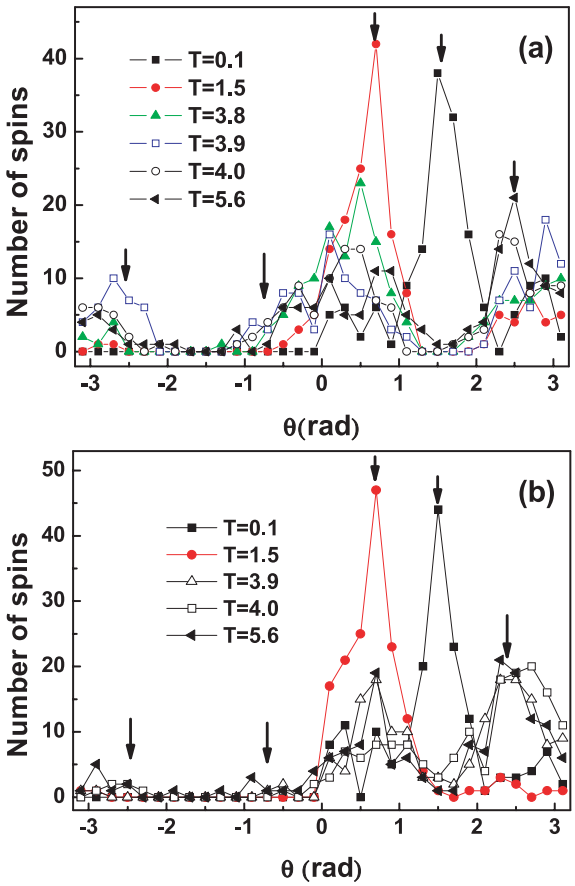

Fig. 8. Spin orientation distributions at different temperatures corresponding to the thermal magnetization in Figure 6b, (a) for $K_b = 0.2$; (b) for $K_b = 1.0$.

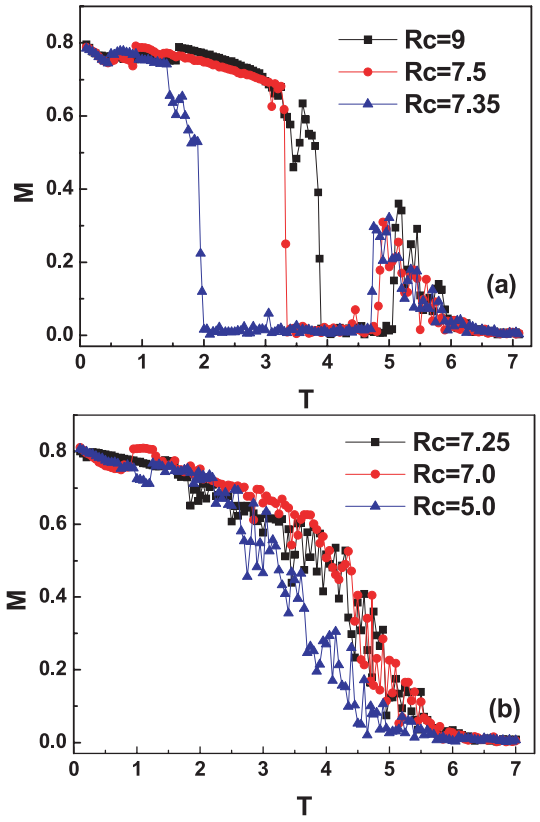

Fig. 9. The thermal magnetizations of the clusters with $K_b = 0$, $K_s = 10$, (a) for $R_c = 9.0$, 7.5, 7.35; (b) for 7.25, 7.0 and 5.0, respectively.

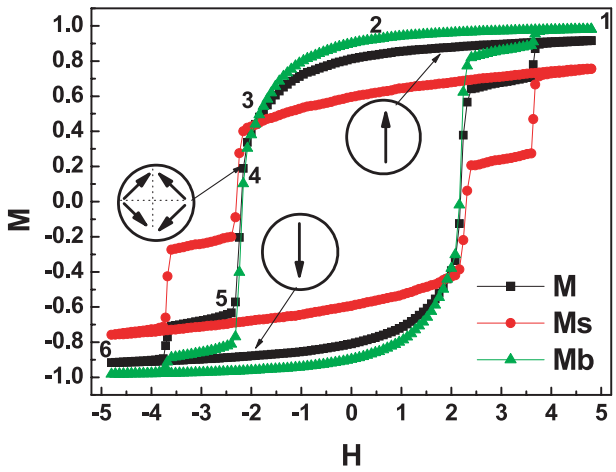

Fig. 10. The typical hysteresis loops of the surface, core and total cluster with $N = 2123$ and $K_b = 0$, $K_s = 10$ at $T = 0.01$, respectively.

degree of spins are more than that in the region (III). Comparing Figure 8a with Figure 8b, we can find that the spin orientation distributions for $K_b = 1.0$ in regions (I), (II) and (IV) are similar to those for $K_b = 0.2$. The difference between both cases above is that the first order transition and multidomain region disappear for $K_b = 1.0$. The thermal magnetizations of the clusters with different extra atoms on the surface along different orientation have been simulated. It is observed that the surface roughness has an important influence on the spin configurations and magnetization behavior. Figure 6b shows only a typical sample and the detailed results will be published elsewhere. In addition, the thermal magnetizations of the clusters with $K_s = 10$ for $R_c = 9.0$, 7.5, 7.35, 7.25, 7.0 and 5.0 (or in the number of atoms, $N = 1505$, 935, 887, 791, 683, 249) are shown in Figures 9a and 9b, respectively. It is seen that the size of the cluster also affects evidently the thermal magnetization behavior, and there exists a critical size R_{cri} (=7.30). As $R_c > R_{cri}$, the first order phase transition emerges. In conclusion, for the above ferromagnetic clusters coated by the surface shell with the surface anisotropy, there exist the critical temperature, surface and core anisotropy and size for the first order phase transition from the single domain to the multidomain.

3.2 Hysteresis loop and coercivity

Figure 10 shows the typical hysteresis loops in the surface, core and total cluster for $N = 2123$ with $K_b = 0$, $K_s = 10$ at $T = 0.01$, respectively. The spin configurations at different magnetization levels corresponding to the loops in Figure 10 are shown in Figure 11. From Figures 10 and 11, it is found that the surface magnetization

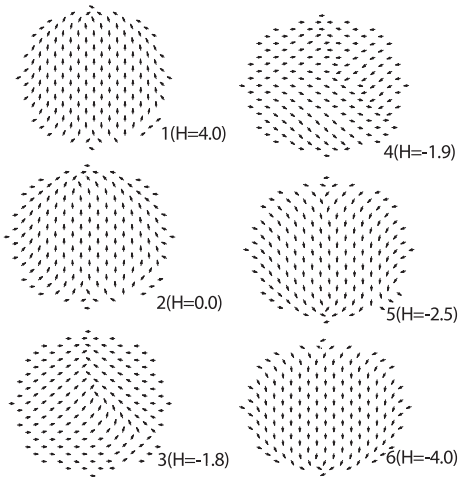

Fig. 11. The spin configurations at different magnetization levels corresponding to the loops in Figure 8.

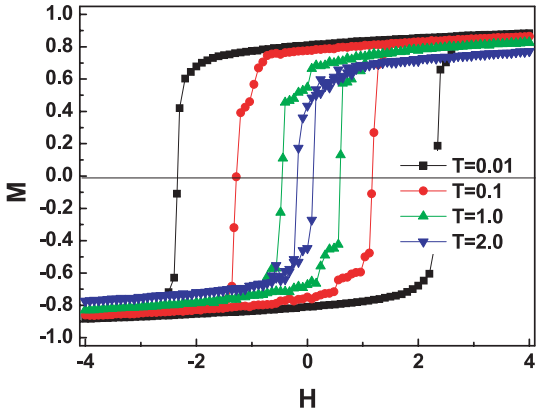

Fig. 12. The typical surface, core and total hysteresis loops of cluster with $N = 249$, $K_b = 0$ and $K_s = 10$ at $T = 0.01$, 0.4, 1.0 and 2.0, respectively.

is difficult to saturate even at very strong fields due to the strong surface anisotropy while the core spins are easy to get saturation, which is a typical feature of the surface with the disordered or frustrated spins [1,4,5]. The spins of the surface tends to lag behind the core spins, reversing more slowly than ones of the core, and requiring greater external magnetic field to reach saturation. This can be considered to be a result of the reduced coordination number and associated weaker effective exchange coupling for the spins of the surface, causing those spins to be localized more by the surface anisotropy. It is worthwhile to note that the spin reversal process can take place in steps with each step related to a particular set of spins reversing. Now, we use the spin configurations as seen in Figure 11 to explain further the magnetization behavior in steps. At the state '1' ($H = 4.0$), the spins in the core align along z axis while those in the surface are forced to rotate towards the direction of the external field. At the state '2' ($H = 0.0$), the spins in the core align still along z axis but the surface spins become disorder after losing the force of the external field. At the states '3' and '4' ($H = -1.8$ and -1.9), the multidomain in which the spins of each subdomain are along two symmetric easy axes of the configurational anisotropy emerges, which is similar to that in Figure 5c ($T = 4.0$). This indicates that the external field can also give rise to a sudden phase transition, which leads to an evident step. At state '5' (such as $H = -2.5$), the core spins reverse to negative z axis while the surface spins remain almost the configuration of the state '4'. Of course, the surface magnetization decreases linearly with decreasing the external field due to the slow titling of the spins whose anisotropy axes deviates from the magnetic field. The state '6' is at negative saturation and similar to the state '1'. In addition, one can note that the break between the states '5' and '6' corresponds to some spins reversing along their anisotropy axes. The steps on hysteresis curves can be explained as follows [14]: the irregular distribution of the surface spins close to reversal creates different potential barriers for different groups of spins in the surface to overcome towards their equilibrium distribution at high field. Relaxing the different groups of surface spins leads to steps in the surface magnetization. The step behavior should relate to the coordination number of the spin.

The thermal coercivity of the magnetic particles has been an interesting subject for a long time in experiment and theory [33–41]. In general, the thermal coercivity can be described by

$$H_c(T) = H_c(0)(1 - C_\alpha T^\alpha) \tag{2}$$

where $H_c(0)$ is the coercivity at $T = 0$ K, c_α is the parameter related to the anisotropy, the volume of the particle and the measuring time. The exponent has a magnitude of $\alpha = 0.5$ for an assembly of aligned particles with single domain and $\alpha = 0.75$ for randomly oriented particles with single domain [33–36]. The hysteresis loops of the clusters with $K_b = 0$, 0.4, 1 and $K_s = 10$ at different temperature have been calculated. Figure 12 shows the typical hysteresis loops of the surface, the core and total cluster with $N = 249$, $K_b = 0$ and $K_s = 10$ at $T = 0.01$, 0.4, 1.0 and 2.0, respectively. From the figure, the magnetization behavior with steps is also found. Figures 13a and 13b show the simulated thermal coercivity for the clusters for $N = 2123$ and 249 with $K_b = 0$, 0.4, 1, $K_s = 10$, and their fitted curves with T^α law, respectively. From the figures, it is found that the temperature dependence of the coercivities of the clusters with $K_s = 10$ can be described by T^α law, except for the high temperature region for $N = 249$. The simulated α values are described as follow: for $N = 2123$, as $K_b = 0$, 0.4, 1.0, $\alpha = 0.2$, 0.1, 0.17, respectively; for $N = 249$, as $K_b = 0$, 0.4, 1.0, $\alpha = 0.3$, 0.3, 0.5, respectively. Those thermal coercivity behaviors are different from the simulated results with $K_s = 0$ [24]. It is obtained that the values of α for the magnetic thin films with the thickness 20 and 6 nm are 1.0 and 0.67 [37], respectively. However, the coercivities of the nanostructured particles such as the ultra-fine iron particles [38], nanometer sized iron clusters [39], γ-Fe_2O_3 nanoparticles [40] and $Co_{0.2}Zn_{0.8}$-Fe_2O_4 spinel oxide [41], reduce drastically with increasing temperature in low temperature region, which trends to fit the T^α law with lower magnitude of α. Therefore, for the cluster with

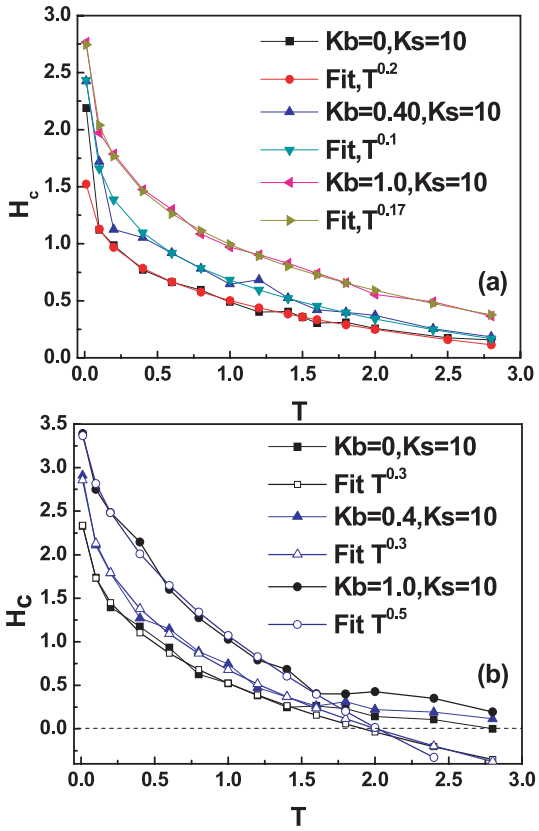

Fig. 13. The simulated thermal coercivity for the clusters with $K_b = 0$, 0.4, 1, $K_s = 10$, and their fitted curves with T^α law, (a) for $N = 2123$; (b) for $N = 249$.

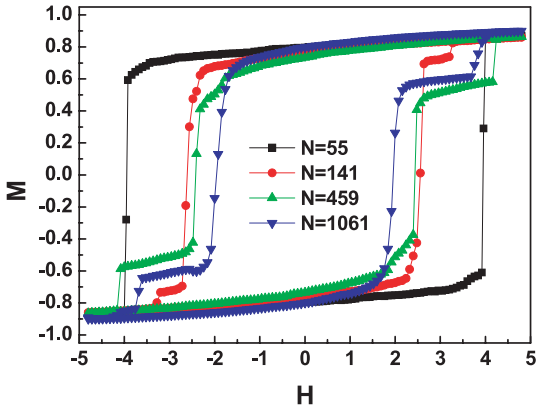

Fig. 14. The hysteresis loops of the clusters for $N = 55$, 141, 459 and 1061 with $K_b = 0$, $K_s = 10$ at $T = 0.01$, respectively.

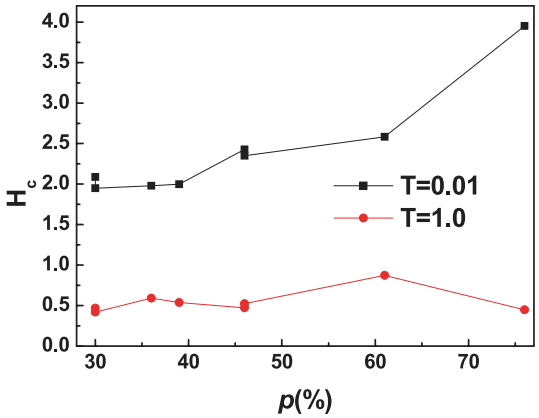

Fig. 15. The p dependence of the coercivity for $N = 2123$ with $K_b = 0$, $K_s = 10$ at $T = 0.01$ and 1.0, respectively.

the complex surface magnetic state, our simulated results with small value of α are consistent with the experimental those of the nanoparticles. Moreover, there exists a cross-point T_{cro} between the thermal coercive curve of the small size ($N = 249$) and that of the large size ($N = 2123$) as seen in Figure 13. As $T < T_{cro}$, the value of H_c for the small cluster with $N = 249$ and $K_s = 10$ is more than that for the large cluster with $N = 2123$ and $K_s = 10$ while the contrary conclusion is obtained as $T > T_{cro}$, which is accordant with the thermal coercivity of the small magnetic particles coated by oxide [35].

3.3 Size and surface effects of hysteresis loops

Figure 14 shows the hysteresis loops of the clusters for $N = 55$, 141, 459 and 1061 with $K_b = 0$, $K_s = 10$ at $T = 0.01$, respectively. The change in shape of the hysteresis loops with the cluster size demonstrates that the reversal mode is strongly influenced by the reduced coordination and disorder in the surface. For the cluster with different size, the ratio p of the number of the surface spins to total those can be obtained. In general, the magnitude of p increases with reducing size. The p dependence of the coercivity for the clusters with $K_b = 0$, $K_s = 10$ at $T = 0.01$ and 1.0 is shown in Figure 15, respectively. From the figure, it is found that the value of H_c increases with the magnitude of p at $T = 0.01$ while at $T = 1.0$ the value of H_c remains nearly unchanged except at $p = 0.62$, which is consistent with the size dependence of the coercivity solved by Landau-Lifshitz equation [14].

Now, let us consider the influence of the surface thickness with the radial anisotropy on the hysteresis loops. It is assumed that the thickness of the surface layer $D = R_c - R_{core}$ is changed, as seen in Figure 1. For the same size (such as $N = 2123$ or $R_c = 10$), the core size decreases with increasing value of D. Figures 16a and 16b show the typical total hysteresis loops with $N = 2123$, $K_b = 0$, $K_s = 10$, $D = 2.0$, 4.0, respectively. From the figures, it is found that the magnitude of H_c and the number of steps increase with the value of D. Also, it is seen that the core loops are quite square while the magnetization with the little step is produced for finite value of D due to the correlation between the surface and core spins. Figure 17 shows the total, core and surface coercivities as a function of D for cluster with $N = 2123$, $K_b = 0$, $K_s = 10$, $T = 0.01$. From the figure, it is observed that, as $D \leq 1$, the total, core and surface coercivities are almost equal; as $1 < D \leq 3$, the total and core coercivities are also equal while the surface coercivity increases greatly; as $3 < D \leq 5$, the total coercivity enhances suddenly, being near to the surface coercivity at $D = 5.0$; as $D > 5.0$,

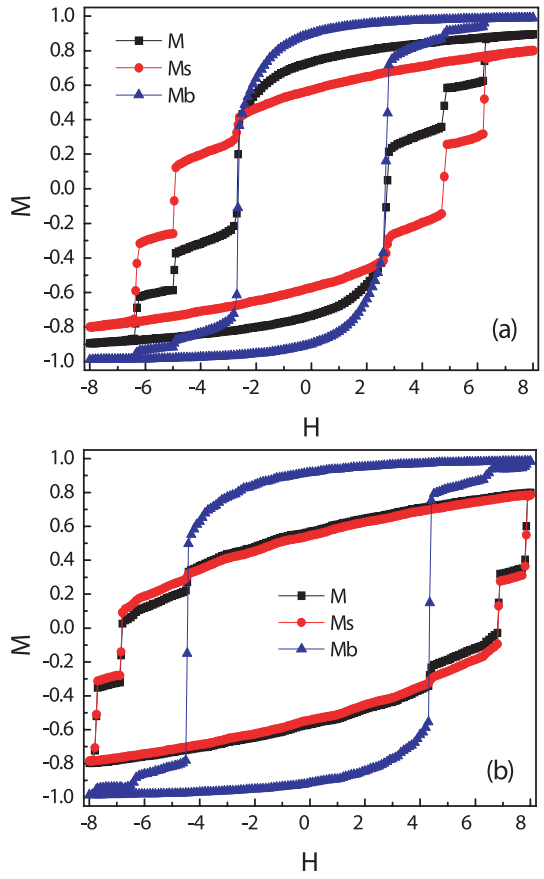

Fig. 16. The typical whole hysteresis loops of the clusters with $N = 2123$, $K_b = 0$, $K_s = 10$, (a) for $D = 2.0$; (b) for $D = 4.0$, respectively.

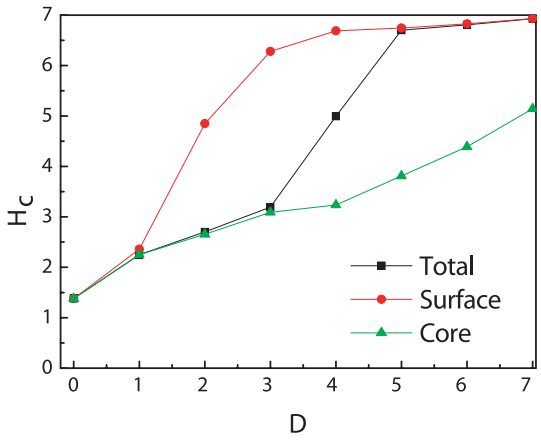

Fig. 17. The total, core and surface coercivities as a function of D for cluster with $N = 2123$ and $K_b = 0$, $K_s = 10$ at $T = 0.01$.

the total and surface coercivities reach saturation but the core coercivity continues to increase linearly. From the above analysis, we can find that the surface plays more important role with increasing surface thickness. The core coercivity decreases with increasing core size (or naming decreasing surface thickness), which is similar to that as seen in Figure 15. This is because the increased mean coordination number for the larger core size favors the collective motion of the spins parallel to each other and results in a smaller coercivity.

4 Conclusions

The magnetic properties of the clusters coated by the surface with the anisotropy are studied by Monte Carlo method. The emphasis is to consider how the cluster size and the magnitude of surface anisotropy influence the spin configuration, thermal magnetization and hysteresis loop. The main features observed are described as follows: (1) the new multidomain containing a few of subdomains whose easy directions are along two symmetric easy axes of the configurational anisotropy is found; (2) the spin reversal process in steps with each step related to a particular set of spins reversing can take place; (3) the first order phase transition from the single domain to the multidomain in the thermal and field magnetization processes is observed, and there exist the critical temperature, the critical surface anisotropy and the critical size in this transition; (4) for the cluster with $K_b = 0$, 0.4, 1, $K_s = 10$, $N = 2123$ and 249, the thermal coercivity can be fitted by $H_c(T) = H_c(0)(1 - C_\alpha T^\alpha)$, which is consistent with the experimental results of the nanoparticles; (5) the hysteresis shapes and coercivity are strongly influenced by the cluster size and the thickness of the surface layer with large anisotropy.

This work was supported by National Key Project for Basic Research of China (No.2005CB623605), NSF of Fujian Province (E0320002, 2005K020), NSF of China under Grant No.10474037.

References

1. R.H. Kodama, A.E. Berkowitz, Phys. Rev. Lett. **77**, 394 (1996); R.H. Kodama, A.E. Berkowitz, J. Appl. Phys. **81**, 5552 (1997); R.H. Kodama, A.E. Berkowitz, Phys. Rev. B **59**, 6321 (1999)
2. K. Haneda, Can. J. Phys. **65**, 1233 (1987)
3. J.M.D. Coey, Phys. Rev. Lett. **27**, 1140 (1971)
4. P. Prene et al., Hyperfine Interactions **93**, 1049 (1994)
5. J.P. Chen, C.M. Sorensen, K.J. Klabunde, G.C. Hadjipanayis, Phys. Rev. B **51**, 11527 (1995)
6. R.D. Zysler, H. Romero, C.A. Ramos, E. De Biasi, D. Fiorani, J. Magn. Magn. Mater. **266**, 233 (2003)
7. E. De Biasi, C.A. Ramos, R.D. Zysler, Phys. Rev. B **65**, 233 (2003)
8. B. Heinrich, B.K. Urguhart, A.S. Arrott, J.F. Cochran, K. Myrtle, S.T. Purcell, Phys. Rev. Lett. **59**, 2464 (1987)
9. S.T. Purcell, B. Heinrich, A.S. Arrott, J. Appl. Phys. **64**, 5337 (1988)
10. G.S. Gay, R. Richter, Phys. Rev. Lett. **56**, 2728 (1986)
11. J.P. Chen, C.M. Sorensen, K.J. Klabunde, G.C. Hadjipanayis, J. Appl. Phys. **76**, 6316 (1994)
12. F. Bodker, S. Morup, S. Linderoth, Phys. Rev. Lett. **72**, 282 (1994)

13. T. Kaneyoshi, J. Phys.: Condens. Matter **3,** 4497 (1991)
14. D.A. Dimitrov, G.M. Wysin, Phys. Rev. B **51**, 11947 (1995)
15. Per-Anker Lindgard, P.V. Hendriksen, Phys. Rev. B **49**, 12291 (1994)
16. K.B. Urquhart, B. Heinrich, J.F. Cochran, A.S. Arrot, K. Myrtle, J. Appl. Phys. **64**, 5334 (1988)
17. Z.S. Shan, D.J. Sellmyer, S.S. Jaswal, Y.J. Wang, J.X. Shen, Phys. Rev. Lett. **63**, 449 (1989)
18. M. Dimian, H. Kachkachi, J. Appl. Phys. **91**, 7625 (2002)
19. Y. Labaye, O. Crisan, L. Berger, J.M. Greneche, J.M.D. Coey, J. Appl. Phys. **91**, 8715 (2002)
20. H. Kachkachi, M. Dimian, Phys. Rev. B **66**, 174419 (2002)
21. O. Iglesias, A. Labarta, Physica B **343**, 286 (2004)
22. L. Hernandez, C. Pinettes, J. Magn. Magn. Mater. **295**, 82 (2005)
23. D.A. Dimitrov, G.M. Wysin, Phys. Rev. B **50**, 3077 (1994)
24. Zhigao Huang, Zhigao Chen, Fengming Zhang, Youwei Du, Eur. Phys. J. B **37**, 177 (2004)
25. Zhigao Huang, Youwei Du, Phys. Lett. A **300**, 641 (2002)
26. S.T. Chui, T. De-Cheng, J. Appl. Phys. **78**, 3965 (1995)
27. X. Zianni, K.N. Trohidou, J. Appl. Phys. **85**, 1050 (1999)
28. K. Binder, D.W. Heermann, *Monte Carlo Simulation in Statistical Physics* (Springer, Berlin, 1992)
29. M.E. Schabes, H.N. Bertram, J. Appl. Phys. **64**, 1347 (1988)
30. L. Torres, E. Martinez, L. Lopez-Diaz, J. Iniguez, J. Appl. Phys. **89**, 7585 (2001)
31. R.P. Cowburn, J. Phys. D: Appl. Phys. **33**, R1 (2000)
32. R.P. Cowburn, A.O. Adeyeye, M.E. Welland, Phys. Rev. Lett. **81**, 5414(1998)
33. H. Pfeiffer, W. Schuppel, Phys. Status Solidi A **119**, 259 (1990)
34. J. Garcia-Otero, A.J. garcia-Bastida, J. Rivas, J. Magn. Magn. Mater. **189**, 377 (1998)
35. K.N. Trohidou, C.M. Soukoulis, A. Kostikas, G. Hadjipanayis, J. Magn. Magn. Mater. **104–107**, 1587 (1992)
36. S.M. Stinnett, J.W. Harrell, A.F. Khapikov, W.D. Doyle, IEEE Trans. on Magn. **36**, 148 (2000)
37. A. Ajan, E.N. Abarra, B.R. Acharya, A. Inomata, I. Okamoto, M. Shinohara, Appl. Phys. Lett. **82**, 1075 (2003)
38. S.U. Jen, C.Y. Lee, Y.D. Yao, J. Magn. Magn. Mater. **96**, 82 (1991)
39. C. Johansson, T. Aklint, M. Hanson, M. Andersson, N. Tarras-Wahlberg, E. Olsson, B. Kalska, R. Wappling, A. Rosen, Nanostructureed Materials **12**, 287 (1999)
40. B. Martinez, A. Roig, X. Obradors, E. Molins, J. Appl. Phys. **79**, 2580 (1996)
41. B.N. Bhowmik, R. Ranganathan, J. Magn. Magn. Mater. **248**, 101 (2002)